Available online at www.sciencedirect.com
SCIENCE DIRECT®
Journal of Sound and Vibration 260 (2003) 167–182
JOURNAL OF SOUND AND VIBRATION
www.elsevier.com/locate/jsvi

Letter to the Editor

Stability analysis of a turbine rotor system with Alford forces

Heung Soo Kim[a], Maenghyo Cho[b], Seung Jin Song[b,*]

[a] *Department of Mechanical and Aerospace Engineering, Arizona State University, Tempe, AZ 85287-6106, USA*
[b] *School of Mechanical and Aerospace Engineering, Seoul National University, Seoul 151-742, South Korea*

Received 29 January 2002; accepted 4 March 2002

1. Introduction

Structural vibration limits the performance of turbomachinery in various applications (e.g., power generation equipment and rocket engine turbopumps). Vibration of structure can be divided into forced and self-excited vibrations, depending on the energy source. In the latter kind, the vibratory motion itself extracts energy from sources (e.g., wind, steam, etc.), leading to instability. Inability to predict these instabilities during the design stage leads to costly delays and shutdowns after installation.

Many sources of self-excited vibrations in rotor systems (e.g., asymmetric bearing stiffness and non-axisymmetric clearance in labyrinth seals) have been identified and extensively analyzed by investigators such as Childs [1], Benckert and Wachter [2], and Millsaps [3]. However, the rotordynamic forces due to non-axisymmetric clearance in turbines and compressors have received relatively little attention. Recently, elementary models for aerodynamic forces which arise in turbines with non-axisymmetric rotor tip clearance (i.e., Alford force) have been developed by Song and Martinez-Sanchez [4,5].

Furthermore, it is as important to investigate the effects of such forces on the structural response of a rotor system. Therefore, fluid–structure interaction analyses (e.g., aeroelasticity of aircraft structures [6]) are needed. However, such effort with regard to rotordynamic instability has been scarce. Therefore, in this paper, a structural model of a rotor system has been developed and integrated with the turbine flow model to examine the effects of the aerodynamic forces on the structural stability of the rotor system. The scope of this paper is limited to the effects of the Alford force, and analytical/numerical methods have been chosen as methods for investigation.

*Corresponding author. Tel.: 82-2-880-1667; fax: 82-2-883-0179.
E-mail address: sjsong@snu.ac.kr (S.J. Song).

PII: S0022-460X(02)00926-4

2. Model description

2.1. Fluid model

The fluid model is an analytical actuator disc model which has been described in Refs. [4,5]. Therefore, only a brief summary is given here. The model assumes incompressible, inviscid flow and analyzes flow redistribution in a single-stage unshrouded axial turbine with a whirling rotor. The incompressible flow assumption limits the present model to low speed (i.e., low Mach number) flows. The inviscid flow assumption is reasonable because viscous effects are much smaller than inertia effects in high Reynolds number flows. The model can predict the stiffness and damping effects of aerodynamic forces. For the case of an eccentric rotor without whirling, the predicted aerodynamic forces matched experimental data to within 25% [5].

The actuator disc model actually consists of two coupled two-dimensional models. The meridional plane model (Fig. 1) is a blade scale analysis which examines the radial flow redistribution of flow caused by a finite axisymmetric rotor tip gap. This model can predict the amount and the underturning of the tip leakage flow and the interaction of the tip clearance flow with the passage flow. Thus, the radially uniform upstream flow splits into a stream associated the turbine passage (marked by "−") and another associated with the tip clearance (marked by "+"). The results of this analysis are then used as connecting conditions for the radial plane model.

The radial plane model (i.e., radius scale analysis, Fig. 2) examines the azimuthal flow redistribution caused by non-axisymmetric rotor tip clearance. The blade scale results are used as

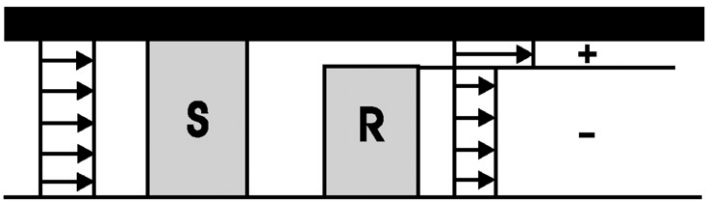

Fig. 1. Blade scale flow model.

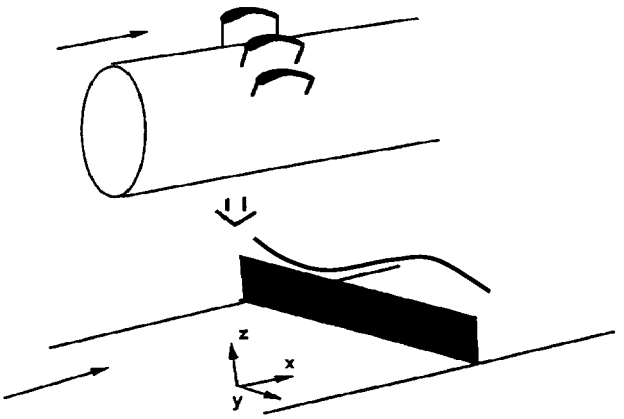

Fig. 2. Radius scale flow model.

the zeroth order solution (i.e., concentric case), and a small perturbation approach is used to examine the eccentric (i.e., non-axisymmetric) case via harmonic analysis. Thus, the perturbations in the tip leakage flow mass fraction, axial and tangential velocities, and pressure are calculated as follows:

$$\begin{bmatrix} \hat{C}_x^+ \\ \hat{C}_y^+ \\ \hat{C}_x^- \\ \hat{C}_y^- \\ \hat{\Delta} \\ \hat{p}/\rho \end{bmatrix}_{x=0+} = \left[\frac{\hat{C}_x(0-)}{U} \frac{\partial}{\partial \phi} + \frac{\hat{C}_y(0-)}{U} \frac{\partial}{\partial \dfrac{C_{y0}}{U}} + \left(\frac{e}{H}\right) \frac{\partial}{\partial \dfrac{t}{H}} \right] \begin{bmatrix} \hat{C}_{x4}^+ \\ \hat{C}_{y4}^+ \\ \hat{C}_{x4}^- \\ \hat{C}_{y4}^- \\ \Delta \\ p_4/\rho \end{bmatrix}. \tag{1}$$

The aerodynamic forces acting on the rotor structure in directions normal and tangent to the instantaneous offset are then determined from the non-axisymmetric pressure and velocity distributions. The aerodynamics forces are given as

$$\langle P \rangle' = P_2' - \frac{P}{2}[\tan^2\beta_3 \bar{C}_{x3}^- \bar{C}_{x3}^{-\prime} - (\bar{C}_{y2} - U)\bar{C}_{y2}'], \tag{2}$$

$$f_y' = \bar{\lambda}\bar{q}_2(\bar{C}_{y2} - \bar{C}_{y3}^+)\left[\frac{\lambda'}{\bar{\lambda}} + \frac{q_2'}{\bar{q}_2} + \frac{C_{y2}' - C_{y3}^+}{\bar{C}_{y2} - \bar{C}_{y3}^+}\right] + (1 - \bar{\lambda})\bar{q}_2(\bar{C}_{y2} - \bar{C}_{y3}^-)\left[\frac{-\lambda'}{1 - \bar{\lambda}} + \frac{q_2'}{\bar{q}_2} + \frac{C_{y2}' - C_{y3}^-}{\bar{C}_{y2} - \bar{C}_{y3}^-}\right]. \tag{3}$$

2.2. Structure model

To develop a structural model of a rotor system, the test rotor system has to be selected first. The test rotor system is shown in Fig. 3. The test rotor system consists of a disc connected to a shaft supported at both ends by bearings. The bearings exert stiffness and damping forces on the shaft, and the disc is equidistant from both bearings. Euler–Bernoulli beam model is used to describe slender shaft. The parametric values of the test rotor system are taken from Childs [1] and are listed in Table 1. Fig. 4 shows the test rotor system with the shaft in its first bending mode. The disc is assumed to be rigid and symmetric ($I_{Dx} = I_{Dy}$). It is also assumed the angle Θ_X and Θ_Y are

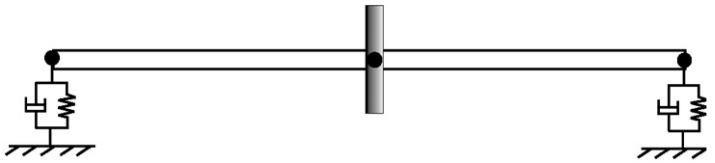

Fig. 3. Test rotor system.

Table 1
Test rotor system parameters

Density of axis	$\rho = 7750\,\mathrm{Kg/m^3}$
Stiffness of axis	$E = 2.036 \times 10^{12}\,\mathrm{N/m}$
Radius of axis	$R_s = 0.028\,\mathrm{m}$
Radius of disc	$R_d = 0.14\,\mathrm{m}$
Thickness of disc	$T_d = 0.024\,\mathrm{m}$
Stiffness of bearing	$K_B = 6.1 \times 10^8\,\mathrm{N/m}$

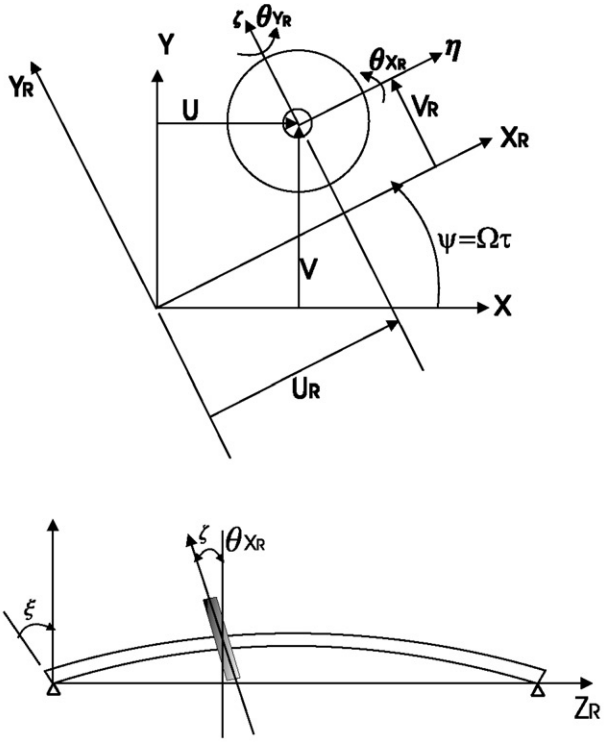

Fig. 4. Schematic of a whirling rotor.

small and the angular velocity is constant ($\dot{\psi} = \Omega$). The dynamics and finite element approach of the single disc rotor system are well known and given as follows [7].

For the disc

$$M_D\ddot{q}_d + C_D\dot{q}_d = 0. \tag{4}$$

For the shaft

$$(M_C + M_S)\ddot{q} + C_S\dot{q} + K_S q = F_{ext}, \tag{5}$$

where

$$[M_D] = \begin{bmatrix} m_d & 0 & 0 & 0 \\ 0 & m_d & 0 & 0 \\ 0 & 0 & I_{Dx} & 0 \\ 0 & 0 & 0 & I_{Dx} \end{bmatrix}, \quad [C_D] = \begin{bmatrix} 0 & 0 & 0 & 0 \\ 0 & 0 & 0 & 2\Omega I_{Dx} \\ 0 & 0 & 0 & 0 \\ 0 & -2\Omega I_{Dx} & 0 & 0 \end{bmatrix},$$

$$q_d = [u, v, \Theta_X, \Theta_Y]^{\mathrm{T}},$$

$$[M_c] = \frac{\rho SL}{420} \begin{bmatrix} 156 & 0 & 0 & -22L & 54 & 0 & 0 & 13L \\ 0 & 156 & 22L & 0 & 0 & 54 & -13L & 0 \\ 0 & 22L & 4L^2 & 0 & 0 & 13L & -3L^2 & 0 \\ -22L & 0 & 0 & 4L^2 & -13L & 0 & 0 & -3L^2 \\ 54 & 0 & 0 & -13L & 156 & 0 & 0 & 22L \\ 0 & 54 & 13L & 0 & 0 & 156 & -22L & 0 \\ 0 & -13L & -3L^2 & 0 & 0 & -22L & 4L^2 & 0 \\ 13L & 0 & 0 & -3L^2 & 22L & 0 & 0 & 4L^2 \end{bmatrix},$$

$$[M_s] = \frac{\rho I}{30L} \begin{bmatrix} 36 & 0 & 0 & -3L & -36 & 0 & 0 & -3L \\ 0 & 36 & 3L & 0 & 0 & -36 & -3L & 0 \\ 0 & 3L & 4L^2 & 0 & 0 & -3L & -L^2 & 0 \\ -3L & 0 & 0 & 4L^2 & 3L & 0 & 0 & -L^2 \\ -36 & 0 & 0 & 3L & 36 & 0 & 0 & 3L \\ 0 & -36 & -3L & 0 & 0 & 36 & -3L & 0 \\ 0 & 3L & -L^2 & 0 & 0 & -3L & 4L^2 & 0 \\ -3L & 0 & 0 & -L^2 & 3L & 0 & 0 & 4L^2 \end{bmatrix},$$

$$[C_s] = \frac{\rho I\Omega}{15L} \begin{bmatrix} 0 & -36 & -3L & 0 & 0 & 36 & -3L & 0 \\ 36 & 0 & 0 & -3L & -36 & 0 & 0 & -3L \\ 3L & 0 & 0 & -4L^2 & -3L & 0 & 0 & L^2 \\ 0 & 3L & 4L^2 & 0 & 0 & -3L & -L^2 & 0 \\ 0 & 36 & 3L & 0 & 0 & -36 & 3L & 0 \\ -36 & 0 & 0 & 3L & 36 & 0 & 0 & 3L \\ 3L & 0 & 0 & L^2 & -3L & 0 & 0 & -4L^2 \\ 0 & 3L & -L^2 & 0 & 0 & -3L & 4L^2 & 0 \end{bmatrix},$$

$$[K_s] = \frac{EI}{L^3}\begin{bmatrix} 12 & 0 & 0 & -6L & -12 & 0 & 0 & -6L \\ 0 & 12 & 6L & 0 & 0 & -12 & 6L & 0 \\ 0 & 6L & 4L^2 & 0 & 0 & -6L & 2L^2 & 0 \\ -6L & 0 & 0 & 4L^2 & 6L & 0 & 0 & 2L^2 \\ -12 & 0 & 0 & 6L & 12 & 0 & 0 & 6L \\ 0 & -12 & -6L & 0 & 0 & 12 & -6L & 0 \\ 0 & 6L & 2L^2 & 0 & 0 & -6L & 4L^2 & 0 \\ -6L & 0 & 0 & 2L^2 & 6L & 0 & 0 & 4L^2 \end{bmatrix},$$

$$\{q\} = [u^1, v^1, \Theta_X^1, \Theta_Y^1, u^2, v^2, \Theta_X^2, \Theta_Y^2]^{\mathrm{T}}. \tag{6}$$

M_D and C_D respectively, represent the classical mass and gyroscopic matrices of the disc. m_d and I_{Dx} are the mass and moment of inertia of the disc, respectively. M is the classical mass matrix of the shaft. M_s and C_s show the influence of rotatory inertia and gyroscopic effect of the shaft, respectively. R is the mass per unit volume, S is the cross-sectional area of the shaft and I is the area moment of inertia of the shaft cross-section about the neutral axis. E is the elastic modulus of the shaft and L is the length of the element. After global assemblage, the dynamics of the disc should be added as the structural unknowns of the center as follows:

$$[M]\{\ddot{q}\} = \begin{bmatrix} \cdot & & & \\ & \cdot & & \\ & & +M_d & \\ & & & \cdot \\ & & & & \cdot \end{bmatrix} \begin{Bmatrix} \cdot \\ \cdot \\ \ddot{q}_{n/2+1} \\ \cdot \\ \cdot \end{Bmatrix}, \quad [C]\{\ddot{q}\} = \begin{bmatrix} \cdot & & & \\ & \cdot & & \\ & & +C_d & \\ & & & \cdot \\ & & & & \cdot \end{bmatrix} \begin{Bmatrix} \cdot \\ \cdot \\ \dot{q}_{n/2+1} \\ \cdot \\ \cdot \end{Bmatrix}. \tag{7}$$

2.3. Fluid–structure model

After the global assemblage and incorporation of forces from the bearings and the Alford force, the governing equation takes the form of

$$[M]\{\ddot{q}\} + [C]\{\dot{q}\} + [K]\{q\} = \vec{F}_{spring} + \vec{F}_{damping} + \vec{F}_{A.F}. \tag{8}$$

Here the bearings' damping and stiffness forces are given as

$$\vec{F}_{spring_{n+1}} = -ku_{n+1}\vec{i} - kv_{n+1}\vec{j}, \quad \vec{F}_{damping_1} = -c\dot{u}_{n+1}\vec{i} - c\dot{v}_{n+1}\vec{j} \tag{9}$$

at node $n+1$.

The Alford force takes the following form:

$$\{F_{A.F_{n/2+1}}\} = -\begin{bmatrix} -B_1 & -A_1 \\ A_1 & -B_1 \end{bmatrix} \begin{Bmatrix} \dot{u}_{n/2+1} \\ \dot{v}_{n/2+1} \end{Bmatrix} - \begin{bmatrix} A_0 & B_0 \\ -B_0 & A_0 \end{bmatrix} \begin{Bmatrix} u_{n/2+1} \\ v_{n/2+1} \end{Bmatrix}. \tag{10}$$

After assembling Alford force and bearing force, the governing equation is expressed as follows:

$$[M]\{\ddot{q}\} + [C + C_B + C_{A.F}]\{\dot{q}\} + [K + K_B + K_{A.F}]\{q\} = 0, \tag{11}$$

where C_B and C_{AF} are the damping matrices of the bearing and Alford force, respectively. Also K_B and K_{AF} are the stiffness matrices of the bearing and Alford force, respectively.

3. Model predictions

The turbine fluid model has been run for a test turbine whose parameters are as shown in Table 2. These are typical of modern high-performance turbines. Since the rotordynamic instability often manifests itself as a subsynchronous whirl, frequencies up to the synchronous frequency in both forward and backward directions have been examined. The aerodynamic forces normal and tangent to the instantaneous rotor offset predicted by the fluid model are shown in Figs. 5 and 6. One can then curve fit the data to extract aerodynamic damping and stiffness factors from

$$F_n = A_1(\Omega e_z) + A_0 e_z, \quad F_t = B_1(\Omega e_z) + B_0 e_z, \tag{12}$$

$$-\begin{Bmatrix} F_X \\ F_Y \end{Bmatrix} = \begin{bmatrix} -B_1 & -A_1 \\ A_1 & -B_1 \end{bmatrix} \begin{Bmatrix} \dot{e}_x \\ \dot{e}_y \end{Bmatrix} + \begin{bmatrix} A_0 & B_0 \\ B_0 & A_0 \end{bmatrix} \begin{Bmatrix} e_x \\ e_y \end{Bmatrix} = [C_{A.F}]\{\dot{\vec{e}}\} + [K_{A.F}]\{\vec{e}\}, \tag{13}$$

The damping and stiffness factors and their dimensions thus determined are listed in Table 3. These factors are then incorporated into Eq. (13). The aerodynamic force data need to be in dimensional form because of the difference in normalization between the fluid model and the structure model.

Next, an eigenvalue analysis can be carried out to determine the stability of the rotor system, and the equations of motion for the rotor system can be solved via time marching method to examine the rotor system's transient behavior. To begin the calculation, a rotor offset equivalent to 1% of the annulus height, is given as the initial condition.

Figs. 7–9 illustrate x and y displacements versus time, whirling trajectory, and eigenvalues for the test rotor system. In this case, the shaft is twice as long as the disc diameter, and external damping is non-existent. Figs. 7 and 8 show clearly that the whirl amplitude increases with time, and this instability is shown in Fig. 9 which shows poles with positive real values.

By introducing external damping, in this case at the bearings, the rotor system can be stabilized. Figs. 10–12 show the rotor system behavior at the neutral stability point with the whirl amplitude approaching a steady state value, and the poles located on the imaginary axis. The amount of external damping required is 3050 Ns/m. Increasing damping beyond this point moves the poles further to left so that whirling is damped out. Thus, the stability boundary for a particular rotor system can be determined.

Table 2
Test turbine parameters

R	Ψ	$\bar{t}/H$	e/H
0.2	1.5	2%	1%

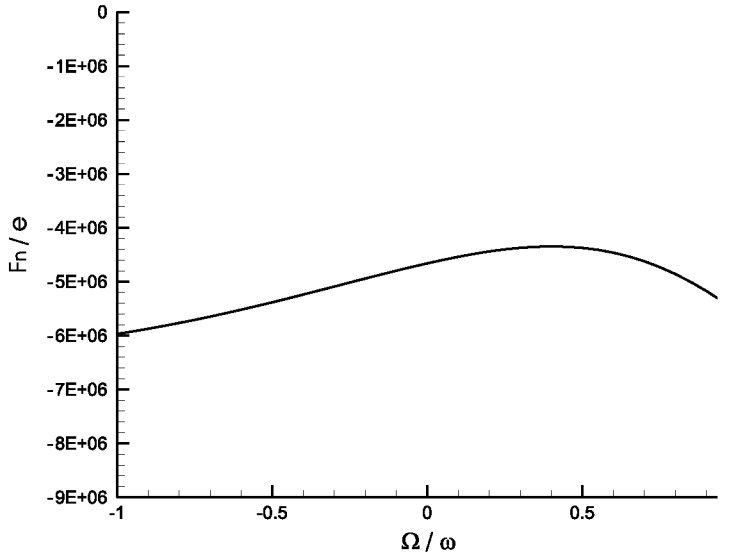

Fig. 5. Aerodynamic force normal to the offset versus whirling frequency.

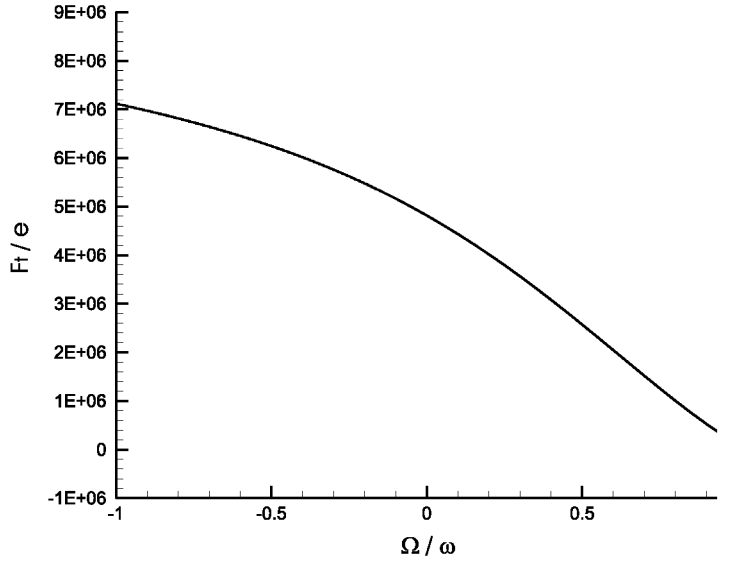

Fig. 6. Aerodynamic force tangent to the offset versus whirling frequency.

Table 3
Aerodynamic damping and stiffness coefficients

	A_1 (Ns/m)	A_0 (N/m)	B_1 (Ns/m)	B_0 (N/m)
$\phi = 0.5$	163.1	−4 628 900	−997	4 762 800

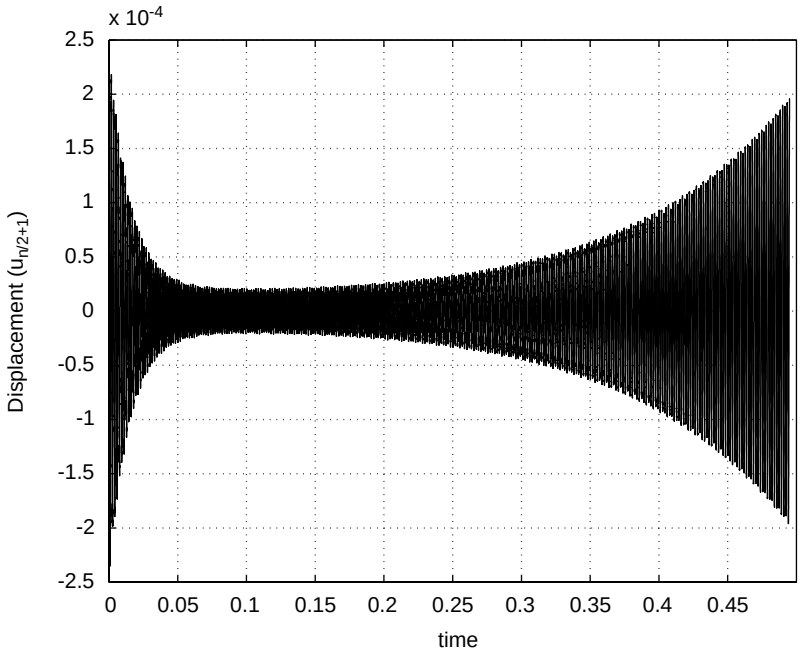

(a) Horizontal displacement vs. time

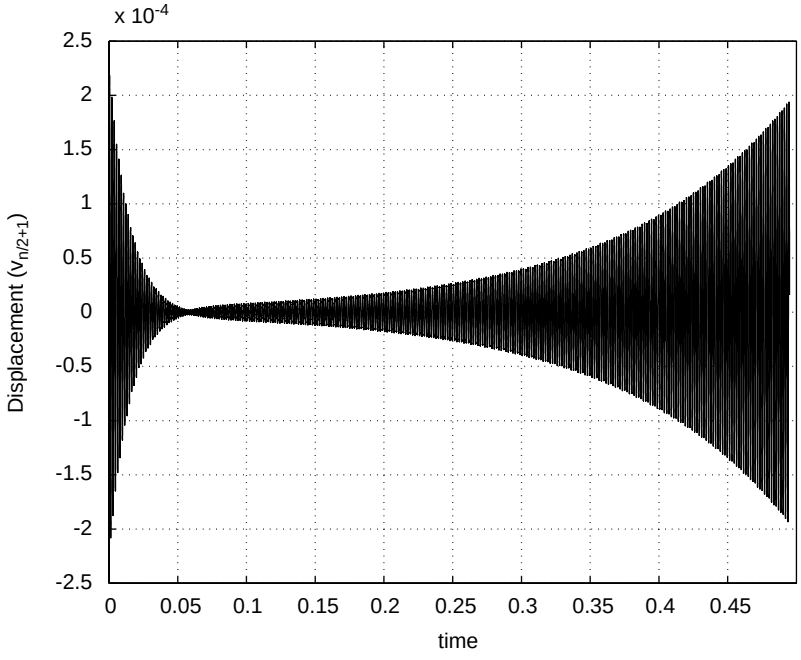

(b) Vertical displacement vs. time

Fig. 7. Displacements versus time without external damping ($L/D = 2.0$).

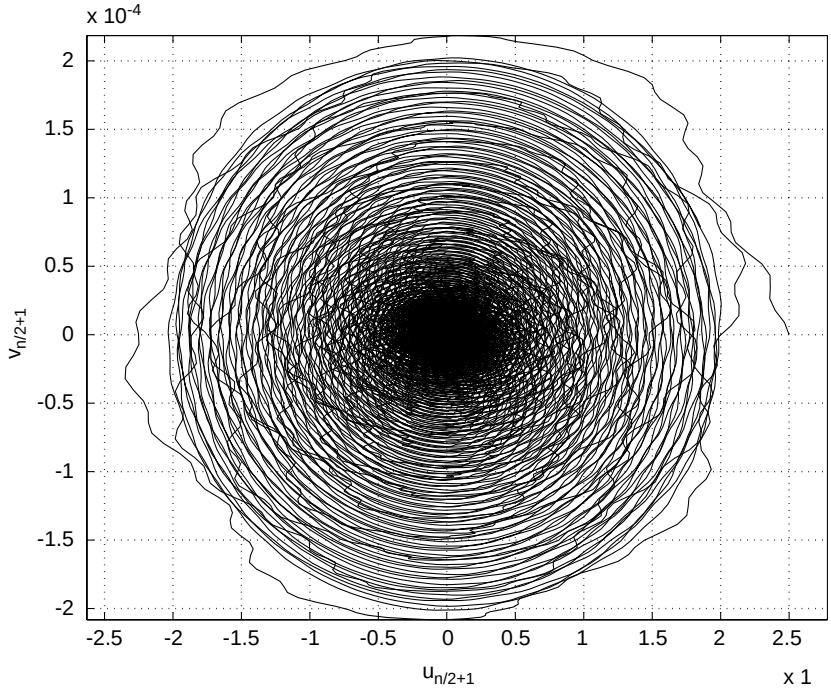

Fig. 8. Whirling orbit versus time.

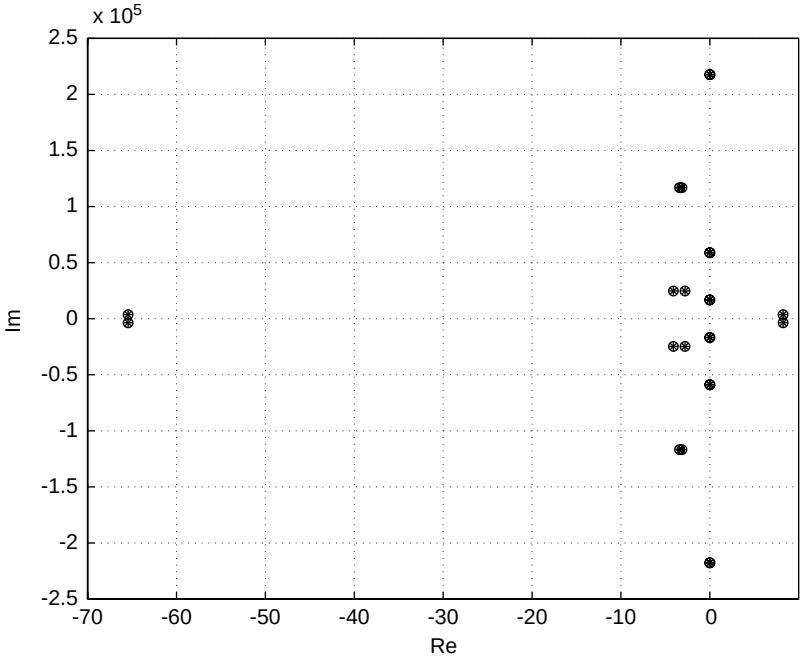

Fig. 9. Root locus plot for the test rotor system without external damping.

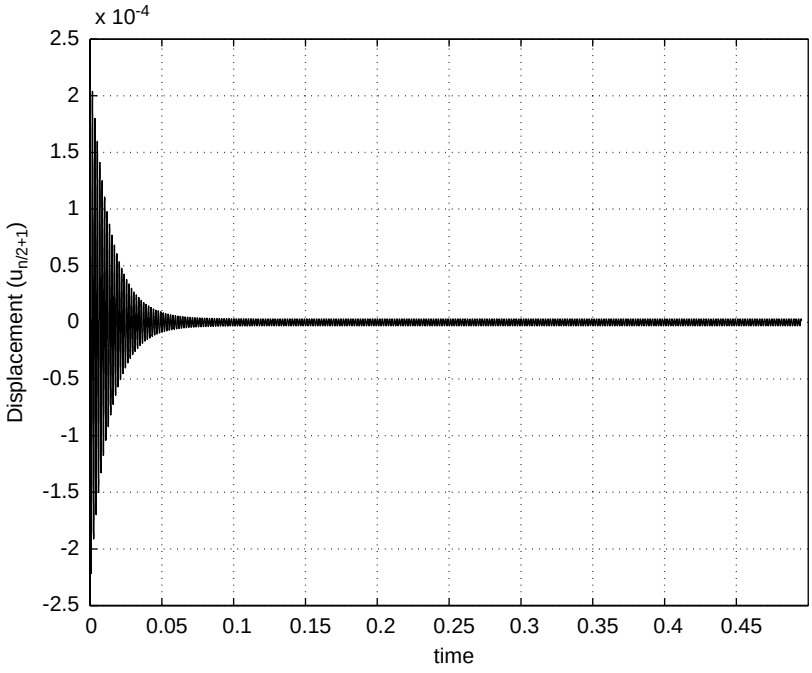

(a) Horizontal displacement vs. time

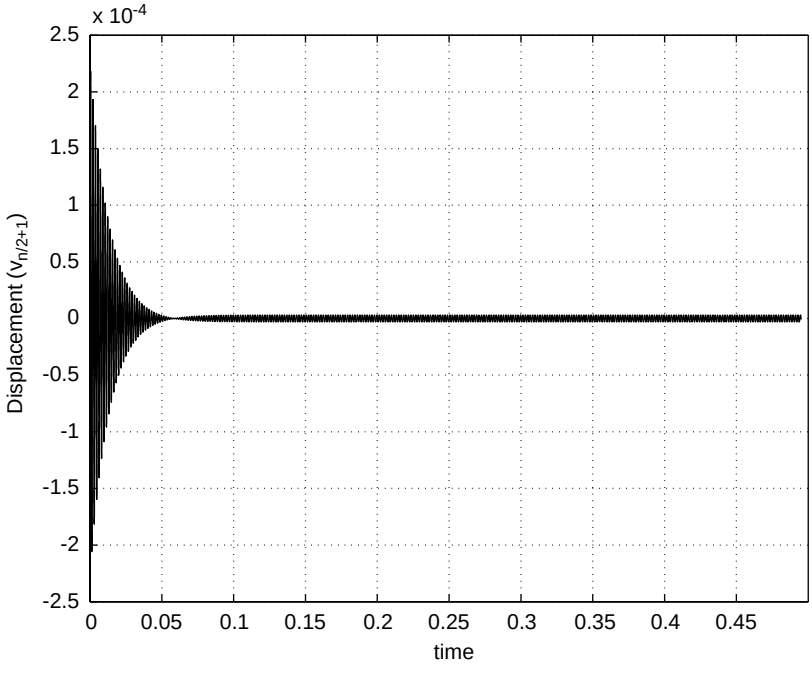

(b) Vertical displacement vs. time

Fig. 10. Displacement *vs*. time with external damping of 3050 Ns/m ($L/D = 2.0$).

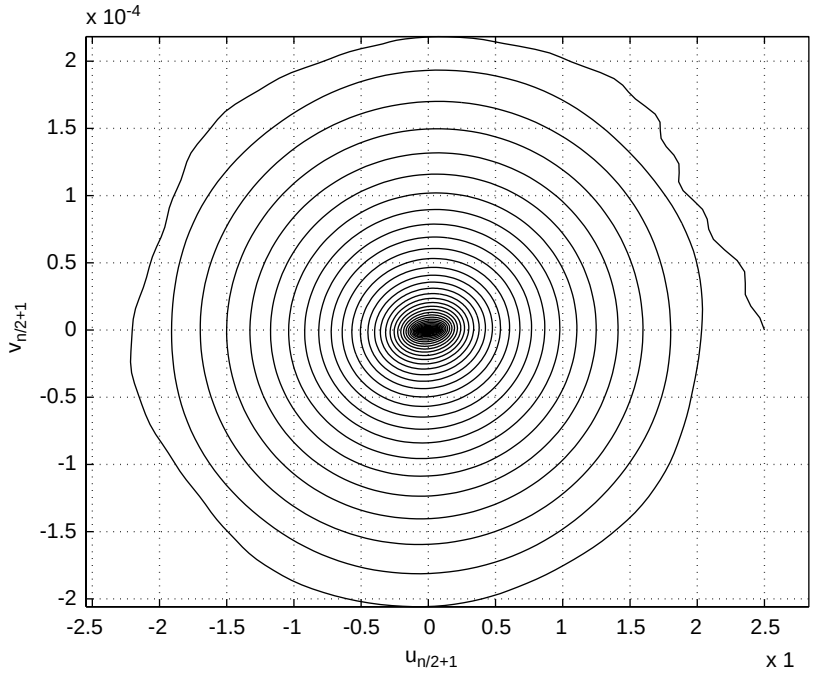

Fig. 11. Whirling orbit versus time.

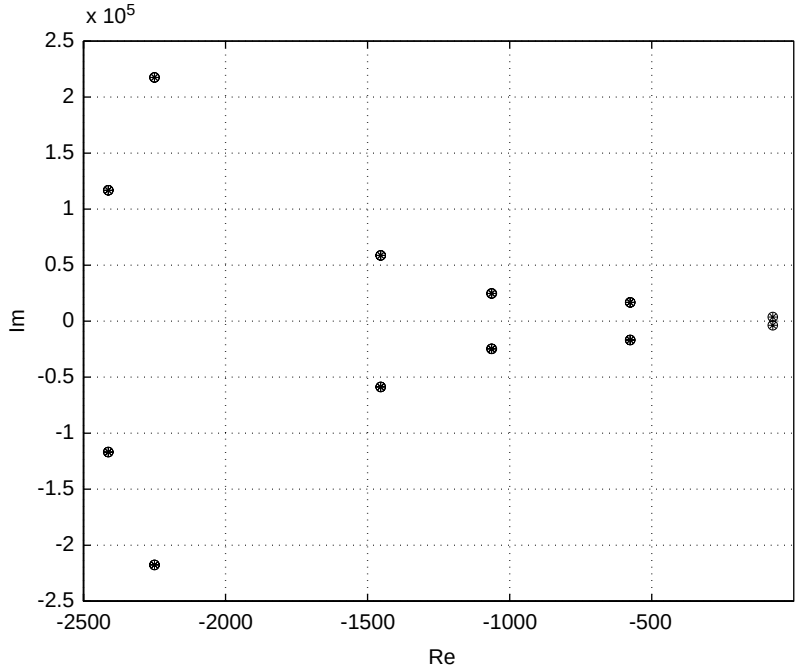

Fig. 12. Root locus plot for the test rotor system with external damping of 3050 Ns/m.

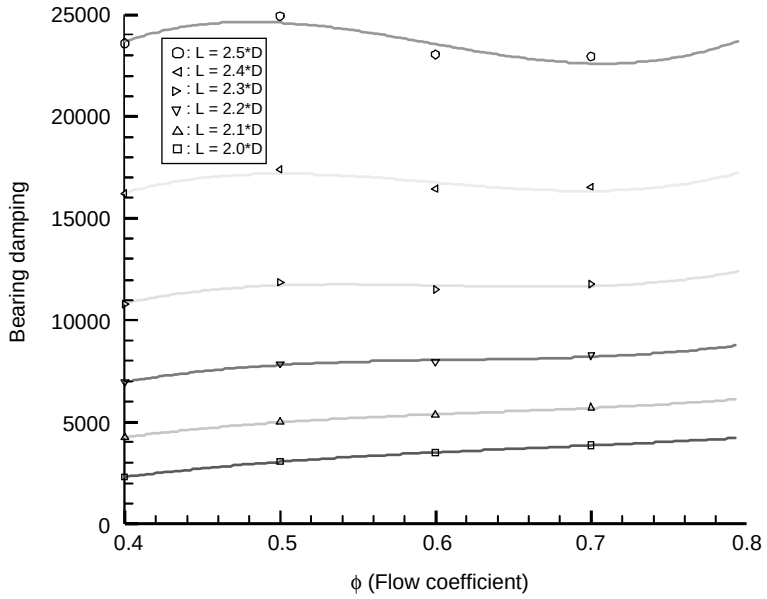

Fig. 13. External damping required for neutral stability versus flow coefficient.

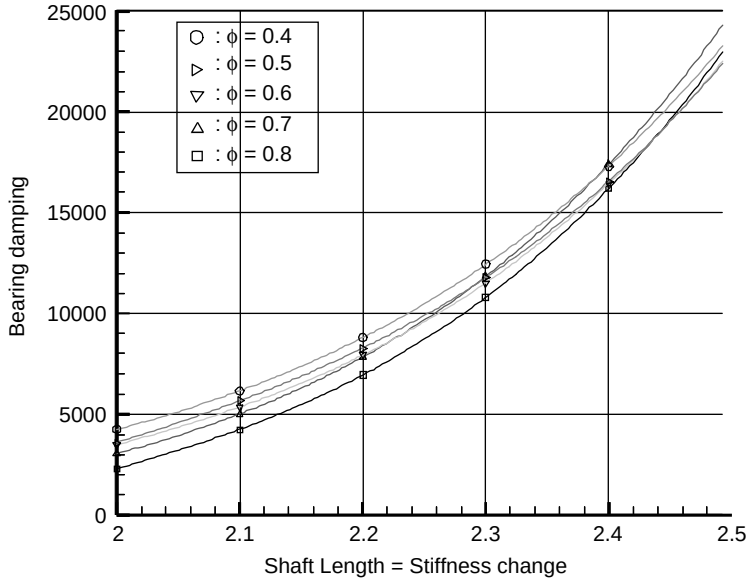

Fig. 14. External damping required for neutral stability versus shaft length.

Using this approach, the effects of flow and geometric parameters have been examined. Specifically, the amount of external damping required for neutral stability for various turbine operating points and shaft lengths has been determined. Fig. 13 shows the required external damping plotted versus the flow coefficient for various shaft lengths. The required external damping is not sensitive to the flow coefficient. Since the stiffness of the shaft is changed according

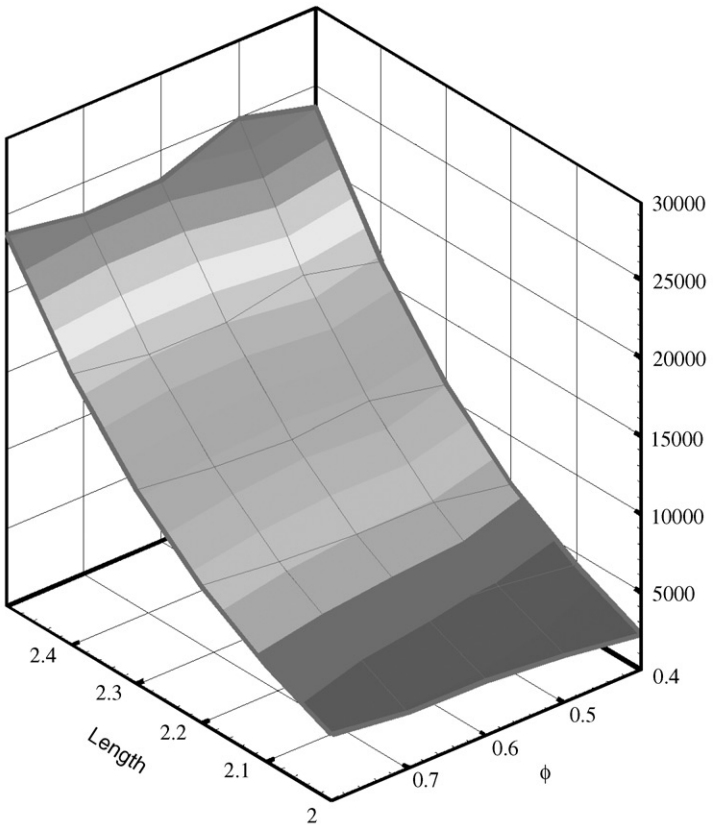

Fig. 15. Stability boundary for varying flow coefficient and the shaft length values.

to the length of the shaft, the change of the stiffness is examined using the variation of the shaft length. A plot of the required external damping versus the stiffness of the shaft (for various flow coefficients) is shown in Fig. 14. The required external damping increases rapidly as the stiffness of the shaft decreases. Increasing shaft length reduces the rotor shaft's lateral stiffness. Therefore, more external damping is required for stabilization. Fig. 15 shows stability boundary of the rotor system according to the variation of the flow coefficient and stiffness of the shaft. The stable single rotor system can be designed using this stability boundary.

4. Conclusions

For the first time, an analytical/numerical stability analysis of a rotor system with Alford effects has been carried out. The Alford force refers to destabilizing lateral aerodynamic forces caused by non-axisymmetric turbine tip clearance. For aerodynamic forces, an actuator disc model, previously developed by Song and Martinez-Sanchez [4,5] was used. In addition, a six-degree-of-freedom model of a rotor system supported at both ends by bearings has been developed. The fluid and structure models were then combined to conduct a fluid–structure interaction analysis. A

classical Euler–Bernoulli beam finite element with support springs and dampers has been employed for structural modeling. The results show that the Alford force can indeed cause structural instability and that external damping can stabilize such a rotor system. Furthermore, the amount of required damping is relatively insensitive to the turbine operating point but increases rapidly as the length of the rotor shaft increases.

Appendix A. Nomenclature

C	absolute velocity
e	eccentricity
f	tangential force acting on the turbine
F	force vector
H	turbine annulus height
I	area moment of inertia
L	element length
K	stiffness matrix
M	mass matrix
p	pressure
q	the strength of vorticity at the interface between tip and passage steams
S	cross−sectional area of the shaft
t	tip clearance
U	turbine rotational speed

Greek letters

β	relative flow angle
Δ	the thickness of the underturned layer
ϕ	turbine flow coefficient
λ	the amount of clearance flow
ρ	mass density
Ω	angular velocity
Θ	rotational angle

Superscripts

.	time derivative
‘	perturbation
$\bar{}$	mean value
^	complex amplitude
+	related to the tip clearance stream
−	related to the passage stream

Subscripts

d	disc
s	shaft

x	axial direction
y	tangential direction
z	radial direction
0	far upstream of turibne
1	turbine stator inlet
2	turbine rotor inlet
3	turbine rotor exit
4	far downstream of turbine rotor

References

[1] D. Childs, Turbomachinery Rotordynamics, Wiley, New York, 1993.
[2] H. Benckert, J. Wachter, Flow induced spring coefficients of labyrinth seals for applications in rotordynamics, NASA CP-2133, 1982, pp. 189–212.
[3] K. Millsaps, The Impact of Unsteady Swirling Flow in a Single Gland Labyrinth Seal on Rotordynamic Stability: Theory and Experiment, Ph.D. Thesis, MIT, Cambridge, MA, 1992.
[4] S.J. Song, M. Martinez-Sanchez, Rotordynamic forces due to turbine tip leakage: Part I — blade scale effects, ASME Journal of Turbomachinery 119 (1997) 695–703.
[5] S.J. Song, M. Martinez-Sanchez, Rotordynamic forces due to turbine tip leakage: Part II — radius scale effects and experimental verification, ASME Journal of Turbomachinery 119 (1997) 704–713.
[6] Dowell, A Modern Course in Aeroelasticity, Kluwer Academic Publishers, Dordrecht, 1995.
[7] M. Lalanne, G. Ferraris, Rotordynamics Prediction in Engineering, Wiley, New York, 1998.